

# Numerical modeling of lander interaction with a low-gravity asteroid regolith surface

## II. Interpreting the successful landing of Hayabusa2 MASCOT

Florian Thuillet<sup>1</sup>, Yun Zhang<sup>1</sup>, Patrick Michel<sup>1</sup>, Jens Biele<sup>2</sup>, Shingo Kameda<sup>3</sup>, Seiji Sugita<sup>4,5</sup>, Eri Tatsumi<sup>4,6</sup>, Stephen R. Schwartz<sup>7</sup>, and Ronald-Louis Ballouz<sup>7</sup>

<sup>1</sup> Université Côte d'Azur, Observatoire de la Côte d'Azur, CNRS, Laboratoire Lagrange, Bd de l'Observatoire, CS 34229, 06304 Nice cedex 4, France  
e-mail: [fthuillet@oca.eu](mailto:fthuillet@oca.eu)

<sup>2</sup> DLR German Aerospace Center, Micro-Gravity User Support Center, 51147 Cologne, Germany

<sup>3</sup> Department of Physics, Rikkyo University, Tokyo, Japan

<sup>4</sup> Department of Earth and Planetary Science, University of Tokyo, 7-3-1 Hongo, Bunkyo-ku, Tokyo 113-0033, Japan

<sup>5</sup> Research Center for the Early Universe, University of Tokyo, 7-3-1 Hongo, Bunkyo-ku, Tokyo 113-0033, Japan

<sup>6</sup> Instituto de Astrofísica de Canarias (IAC), C/Vía Láctea s/n, 38205 La Laguna, Tenerife, Spain

<sup>7</sup> Lunar & Planetary Laboratory, University of Arizona, Tucson, AZ, USA

Received 18 June 2019 / Accepted 18 February 2021

### ABSTRACT

*Context.* The JAXA asteroid sample return mission Hayabusa2 reached its target (162173) Ryugu in June 2018 and released the European (CNES-DLR) lander MASCOT in October 2018. MASCOT successfully landed on the surface, and the Hayabusa2 Optical Navigation Camera system has been able to image parts of the MASCOT trajectory.

*Aims.* This work builds on our previous study of interactions between a landing package and a granular material in the context of MASCOT on Ryugu. The purpose is to expand our knowledge on this topic and to help constrain physical properties of surfaces by considering the actual trajectory of MASCOT and observations of Ryugu from Hayabusa2.

*Methods.* We ran a new campaign of numerical simulations using the  $N$ -body code `pkdgrav` with the soft-sphere discrete element method by expanding the parameter space to characterize the actual landing scenario of MASCOT on Ryugu. The surface was modeled as a granular medium, but we also considered a large boulder in the bed at various depths and a rigid wall representing a cliff. MASCOT was faithfully modeled as the actual lander, and we considered different impact angles, speeds, and surface slopes. We were particularly interested in the outgoing-to-incoming speed ratio of MASCOT during the landing process.

*Results.* We found that a boulder in the bed generally increases both the stochasticity of the outcomes and the speed ratio, with larger increases when the boulder sits closer to the surface. We also found that the surface slope does not affect our previous results and that the impact speed does not affect the speed ratio for moderate-friction granular material. Finally, we found that a speed ratio as low as 0.3, as estimated in the actual scenario, can occur with a solid-rock surface, not only with a soft surface, because the geometry of the lander is nonspherical. This means that we must infer the physical properties of the surface from outcomes such as the speed ratio with caution: it depends on the lander geometry.

**Key words.** minor planets, asteroids: individual: Ryugu – methods: numerical

### 1. Introduction

Hayabusa2 is a Japan Aerospace eXploration Agency (JAXA) asteroid sample return mission toward the C-type near-Earth asteroid (162173) Ryugu (Binzel et al. 2001; Wada et al. 2018). It arrived at Ryugu on June 27, 2018 (Watanabe et al. 2019), and successfully performed a first touch-down and sampling on February 21, 2019, with the goal of returning asteroid material to Earth on December 6, 2020. Before the first touch-down, the Hayabusa2 spacecraft released two mini-rovers called MINERVA-II-1A and B in September 2018 (Van wal et al. 2018, 2019) and the CNES-DLR (French and German space agencies) lander MASCOT (Ho et al. 2017), which safely reached the surface of Ryugu on October 3, 2018. The purpose of MASCOT was to carry out in situ measurements with an imaging spectrometer (Bibring et al. 2017), a camera (Jaumann et al. 2017), a radiometer (Grott et al. 2017), and a magnetometer (Herčík et al. 2017).

MASCOT was safely found by the Optical Navigation Camera Telescope (Kameda et al. 2017) on board the Hayabusa2 spacecraft, and data could be retrieved. In addition to very fruitful in situ measurements of the surface of Ryugu (Jaumann et al. 2019; Grott et al. 2019), supplementary information on the surface properties can be obtained by reconstructing the MASCOT trajectory, and in particular, its bouncing on the asteroid surface.

This study builds on Maurel et al. (2018) and Thuillet et al. (2018), who modeled the landing of MASCOT in a regolith bed with an impact speed of  $19 \text{ cm s}^{-1}$  before the actual landing. We present the results of new simulations here that we performed after the landing occurred. In these simulations, we account for the real morphological features of the MASCOT landing area. Our objective is to investigate the actual landing conditions and determine whether the behavior of MASCOT can allow us to infer some properties of the surface of Ryugu.

**Table 1.** Characteristics and properties of the two material types considered in our simulations (the same as used in [Thuillet et al. 2018](#)).

Material type	Angle of repose ( $^{\circ}$ )	$\varepsilon_n$	$\varepsilon_t$	$\mu_s$	$\mu_r$	$\mu_t$	$\beta$
Gravel-like friction	38.5	0.5	0.5	1.0	1.05	1.3	1.0
Moderate friction	28						0.2

Our knowledge of low-speed impacts on granular media has significantly increased in the past decade. Studies of granular material were initiated to better understand the behavior of this medium on the Earth, with various industrial applications. Furthermore, the discovery that the surfaces of many asteroids are covered with granular material called regolith (which can appear in very different forms and does not necessarily blanket the entire body of an asteroid) initiated a new area of research in planetary science devoted to understanding granular material dynamics on low-gravity bodies. In particular, the development and the proceedings of two sample return missions from asteroids, Hayabusa2 ([Watanabe et al. 2017](#)) and OSIRIS-REx ([Lauretta et al. 2017](#)), were two powerful motors for the activity in this field.

A series of experiments were conducted under Earth gravity ( $1g$ ) for obvious reasons of feasibility. Several characteristics of low-speed impacts on granular materials can be extracted from these experiments, such as the drag-force law stopping the impactor (see, e.g., [Katsuragi & Blum \(2017\)](#) for dust aggregates, [Katsuragi & Durian \(2007\)](#) for glass beads, and [Uehara et al. \(2003\)](#) for several granular media), and properties of the crater that is formed by the impact ([Uehara et al. 2003](#); [Walsh et al. 2003](#); [de Vet & de Bruyn 2007](#)).

However, to better replicate an asteroidal environment, reduced-gravity experiments can be performed on the Earth with Atwood machines ([Murdoch et al. 2017](#)) and parabolic flights ([Colwell et al. 2008, 2015](#)). With these methods, environmental gravity as low as  $10^{-2}g$  can be achieved. Another solution is to perform experiments in space, for example, in the Space Shuttle ([Colwell 2003](#)), where the gravitational acceleration can go down to  $10^{-4}g$ . These experiments showed that the behavior of the impactor can vary depending on the gravity, and that lower gravity incites bouncing ([Brisset et al. 2018](#)).

Numerical simulations provide a way to bypass the gravity problem, as the gravitational field is usually a modifiable parameter. After these modeling frameworks have been validated and calibrated by experiments, they can be a powerful tool for exploring wider parameter spaces under different gravity conditions.

We first introduce the setup of our simulations in Sect. 2, and in Sect. 3 we present the results we obtained for different configurations that could represent what MASCOT experienced. Section 4 presents the conclusions of our investigation.

## 2. Method

This study is the continuation of [Maurel et al. \(2018\)](#) and [Thuillet et al. \(2018\)](#), and most of the parameters used in our simulations are identical. We used the  $N$ -body numerical code `pkdgrav` ([Richardson et al. 2000](#); [Stadel 2001](#); [Richardson et al. 2009, 2011](#)), with the implementation of the Soft-Sphere Discrete Element Method (SSDEM) ([Schwartz et al. 2012](#)). SSDEM allows us to better characterize interactions between grains, such as friction and energy damping, which were later improved by [Zhang et al. \(2017\)](#) using spring-dashpot-slider

models for the twisting and rolling frictions. `pkdgrav` was validated through several comparisons with experiments, such as hopper discharges ([Schwartz et al. 2012](#)), low-speed impacts ([Schwartz et al. 2014](#); [Ballouz 2017](#)), avalanches and angle-of-repose experiments ([Yu et al. 2014](#); [Maurel et al. 2018](#)), and triaxial compression tests ([Zhang et al. 2018](#)).

The setup used in this study is similar to that in [Thuillet et al. \(2018\)](#), that is, a cylinder with a radius of 150 cm filled with grains and the  $\sim 20$  cm lander MASCOT impacting the granular bed at an impact speed of  $19 \text{ cm s}^{-1}$  (except in Sect. 3.4). We generally consider that the regolith bed is 30 cm deep, with a Gaussian size distribution (mean radius of 1 cm, a standard deviation of 33%, and a cutoff at  $1\sigma$ ). The grain size distribution on Ryugu was measured to be a power law with an exponent of  $-2$  to  $-2.5$  ([Sugita et al. 2019](#); [Michikami et al. 2019](#)). The resolution of ONC-T images at the actual MASCOT impact site is  $30 \text{ cm pix}^{-1}$ . Based on these images, it is therefore difficult to determine the exact grain size of the region. The resolution near the impact site is  $6 \text{ cm pix}^{-1}$ , as shown in Fig. S14B in [Sugita et al. \(2019\)](#). This shows that a large portion of the surface is covered with boulders with sizes comparable to or larger than MASCOT. Several patches deposited by regolith grains are much smaller than MASCOT. The size distribution appears to continue down to 10 cm, as shown in Fig. S14A ([Sugita et al. 2019](#)); regoliths consisting of grains smaller than 10 cm near the impact site of MASCOT also exist. Because we do not know how the size distribution may change for 1 cm grains, we assumed a Gaussian distribution, which allowed us to optimize the computational time of our SSDEM simulations and to cover a larger parameter space regarding other properties and impact conditions.

The SSDEM parameters used in our simulations are the same as in [Thuillet et al. \(2018\)](#). The three friction parameters (static  $\mu_s$ , rolling  $\mu_r$ , and twisting  $\mu_t$ ), the shape parameter  $\beta$ , and the restitution coefficients (the main source of energy dissipation) are shown in Table 1. The shape parameter  $\beta$  represents the rotational resistance due to the angularity of grains, even if the grains in our simulations are spherical. When  $\beta = 0$ , the rotational resistance between grains is zero, resembling the contact physics of smoothed spherical particles. The increase in  $\beta$  leads to an increase in rotational resistance, and so it plays an important role in the angle of repose and the friction of the material. A detailed description of the meaning of each coefficient can be found in Sect. 2 in [Zhang et al. \(2017\)](#). We chose two different materials, one with high friction (gravel-like) and another with moderate friction. These materials differ by the shape parameter, that is, by the angularity of the grains. This results in different angles of repose: the highest angle of repose corresponds to the largest angularity.

As in [Maurel et al. \(2018\)](#) and [Thuillet et al. \(2018\)](#), we use “walls”, that is, immobile surfaces, to model the cylinder containing the regolith bed. These walls have the same physical properties as the grains, except that we consider lower restitution coefficients to avoid reflections of impact waves on the walls. We note that the boundary conditions do not seem to

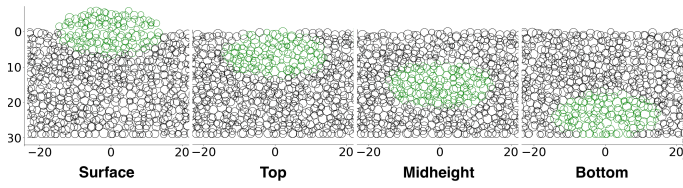


**Fig. 1.** Different vertical positions considered for the boulder. The average particle radius is 1 cm.

affect the outcomes of the impact, particularly on the dynamics of MASCOT (Thuillet et al. 2018).

We modeled MASCOT as a 19.5 cm × 27.5 cm × 29 cm cuboid with a small prominence that represents the hyperspectral microscopic imager MicrOmega (Bibring et al. 2017). In our simulations, MASCOT is made of an assembly of “reactive” walls, that is, walls that can react to contact forces with particles and are therefore affected by the accumulative forces acting on them. The walls are assembled together to represent a rigid body, the MASCOT. The center of gravity, the matrix of inertia, and three principal axes of the assembly can be calculated accordingly. The detailed model parameters of MASCOT are given in Sect. 4.1 in Maurel et al. (2018). The friction coefficients ruling the interactions between MASCOT and the grains are the same as the grain-grain coefficients. However, the restitution coefficients of MASCOT correspond to the structural restitution coefficient measured by Biele et al. (2017), that is, 0.6, and their effect has been investigated in Thuillet et al. (2018). MASCOT does not rotate before impact, and therefore its energy prior to the impact is only translational. For the orientation at landing, we used the three orientations defined by Thuillet et al. (2018) (see their Fig. 1): flat, back corner first, and front corner first.

In this study, we studied the outgoing-to-incoming speed ratio of MASCOT in particular, as a general result with the consideration of several environments and information derived from images taken by the Hayabusa2 Optical Navigation Camera before and after the first bouncing. The speed ratio was also studied in Maurel et al. (2018) and Thuillet et al. (2018), and therefore this enables direct comparisons with previous works. Moreover, because the asteroid surface is not flat and the gravitational field we consider is only locally correct, the speed ratio is more convenient for comparisons with the actual landing.

### 3. Results

In this section, we describe the simulated scenarios and analyze the results. First, we introduce the notion of a boulder in the regolith bed and study its effect on the behavior of MASCOT because we cannot rule out this possibility when MASCOT bounced on the surface of Ryugu. Then, we consider local variations of gravity, either with slopes or with the improved knowledge of the gravity field of Ryugu, and finally, we consider a bounce on a wall representing a vertical side of a high-standing boulder, as suggested by images obtained with the Hayabusa2 Optical Navigation Cameras.

#### 3.1. Effect of a boulder

We first investigate the effect of a boulder buried in the regolith bed. In effect, we cannot rule out the possibility that a boulder was located just below the surface or deeper, and it would be entirely undetectable from the home position of Hayabusa2. Ryugu images showed that some boulders are at least partially

buried (Sugita et al. 2019), and we must thus consider this possibility.

#### 3.1.1. Boulder model and setup

Boulders are modeled as aggregates in pkdgrav as standard particles stuck together, meaning that they behave as a rigid body. We considered ellipsoidal boulders with aspect ratios 1:0.74:0.43, corresponding to the ratios  $\frac{a}{a}$ ,  $\frac{b}{a}$ , and  $\frac{c}{a}$  of the semiaxes  $a$ ,  $b$ , and  $c$ . These ratios are close to those that are usually considered for fragments of catastrophic disruptions 2:  $\sqrt{2}$ :1 (Capaccioni et al. 1984, 1986) and to the mean aspect ratios that have been experimentally observed on fragments resulting from high-energy collisions by Fujiwara et al. (1978) and Durda et al. (2015). These aspect ratios are also very similar to those of the boulders observed on (25143) Itokawa by the Hayabusa mission (Michikami et al. 2016), and to the particles from Itokawa sampled by Hayabusa that were brought back to Earth in 2010 (Tsuchiyama et al. 2014; Michikami et al. 2018).

For the semimajor axis, 30 cm is a critical boulder length because this size is comparable to that of MASCOT, but cannot be detected from the home position of Hayabusa2. Thus, we took 30 cm as the longest dimension of the boulder. The second and third ones are coming directly out of the aspect ratios given before. As a result, the boulders we considered in our simulations consist of grains whose centers are located in a 30 cm × 22.2 cm × 12.9 cm ellipsoid. This is to be compared to the average particle radius of 1 cm. Boulders weight about 5–5.6 kg, and the same bulk density as grains in the bed, i.e., about 1.1–1.3 g cm<sup>-3</sup>. They have the same friction coefficients and coefficients of restitution as individual grains, and react to both grains and MASCOT.

We studied four vertical positions and three horizontal ones for the boulder aggregate. We examined a scenario in which the boulder was at the bottom of the bed (“bottom”), in the middle of it (“midheight”), just below the surface (“top”), or half-buried (“surface”), as shown in Fig. 1. In each simulation, the boulder moves, usually in the same direction as the grains surrounding it.

#### 3.1.2. Boulder at different vertical positions

We first analyze the outcomes for the cases where the boulder is located at the center of the granular bed and the effect of the vertical position of the boulder.

##### (a) Speed ratios of MASCOT

Figure 2 shows the speed ratio  $\frac{V_{out}}{V_{in}}$  obtained for different vertical positions, assuming that MASCOT lands on its back corner first. First, as expected, we note that the higher and closer to the surface of the boulder, the larger the differences with the no-boulder case in general. We find that a boulder located at the bottom of the regolith bed has little to no effect on the speed ratio. As discussed in our previous study (see the discussion in Sect. 3.8 in Thuillet et al. 2018), the stochasticity due to the chaotic nature of granular systems and computational noise could lead to changes in the speed ratio up to 0.1 in the no-boulder case, which is larger than the difference between the no-boulder case and the bottom case in general. The difference in the outcomes would mainly come from stochasticity. For the midheight boulders, we find that generally, the speed ratios are higher than in cases without a boulder or a boulder at the bottom. These differences can be as high as 0.2, corresponding to an outgoing speed difference of about 4 cm s<sup>-1</sup>. Different from the other three cases, which show systematic trends with increasing

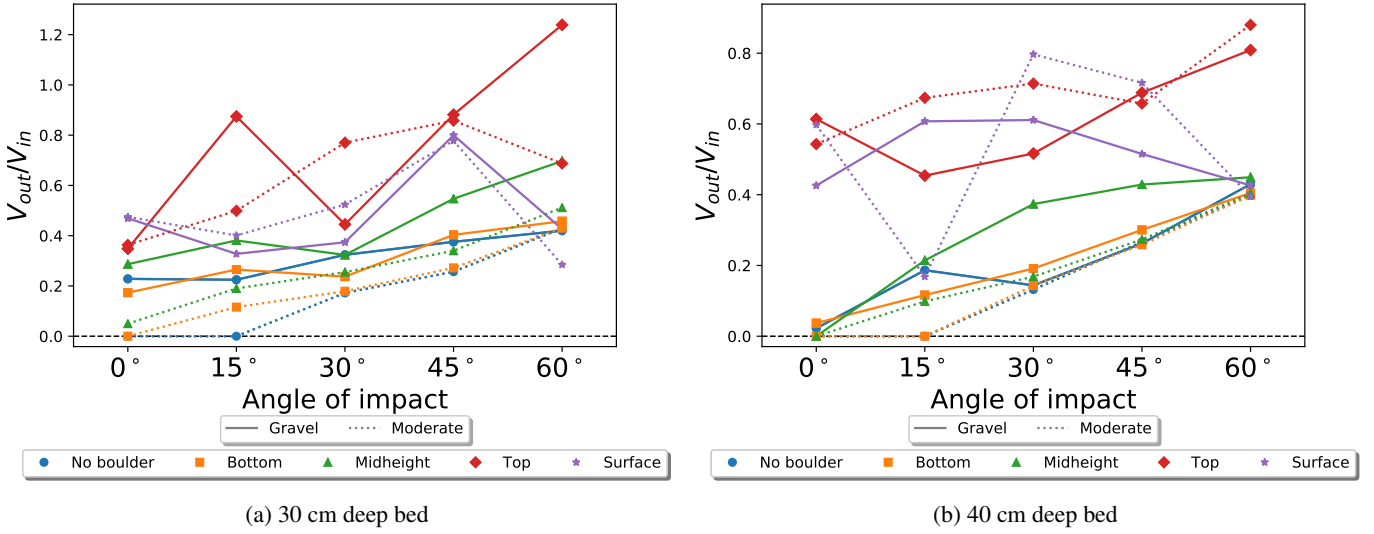


**Fig. 2.** Outgoing-to-incoming speed ratio of the lander as a function of the impact angle ( $0^\circ$  is a normal impact, and larger angles correspond to more grazing impacts), the material friction, and the position of the boulder for a 30 cm bed (*left*) and a 40 cm bed (*right*). The line types represent the frictional properties of the granular bed, and the symbols and colors represent the different boulder positions, as indicated at the bottom. MASCOT lands on its back-corner first in these simulations. Stochasticity due to computational noise could lead to changes in the speed ratio up to 0.1.

impact angle, bed depth, and grain angularity, the top-boulder and surface-boulder cases show a very complex speed ratio function. This is caused by the sensitivity to the contact geometry between MASCOT and the boulder. Due to the irregular shape of the boulder, slight changes in the impact angle, in the bed depth, or in the particle friction could lead to a different contact position and change the direction of the recoil force. Therefore the coupling spin-translational motion of MASCOT is subject to a much larger uncertainty than in the other cases.

For material with moderate friction, the speed ratios for all the cases and the effect of the boulder position are generally lower (except for the top and surface cases), and stochasticity may also play a role in these differences. We also note that on average, the differences due to the boulder position (except for the top and surface cases) are more pronounced for a 30 cm than for a 40 cm bed because the increase in the relative size of the boulder to the bed depth can increase the overall rigidity of the granular bed and emphasize the effect of the boulder.

Figure 3 shows cross-section snapshots of MASCOT impacting the regolith bed containing a buried boulder. If there is no boulder, the particles in contact with the lander are mobilized, and the resulting kinetic energy that is transferred to particles through contact network is propagated to other particles. These mobile particles reduce the resistance of the granular bed to penetration by the lander in general. On the other hand, a boulder increases the resistance to penetration by the boulder into the bed if the boulder is located close enough to the surface, preventing energy transfer to mobilize particles. More kinetic energy is preserved in the lander during its bounce on the boulder. Consequently, a boulder close enough to the impact location increases the outgoing-to-incoming speed ratio.

The highest outgoing speeds for the different vertical boulder locations occur when the boulder is just below the surface (top boulder). Moreover, the outcome is much more stochastic than for the other cases. Whereas we generally find that the speed ratio increases as a function of the impact angle, it is more erratic with a top boulder because MASCOT comes directly into contact with the boulder. In this case, the speed ratios can be even higher than 1. This phenomenon was also found in the experiments of

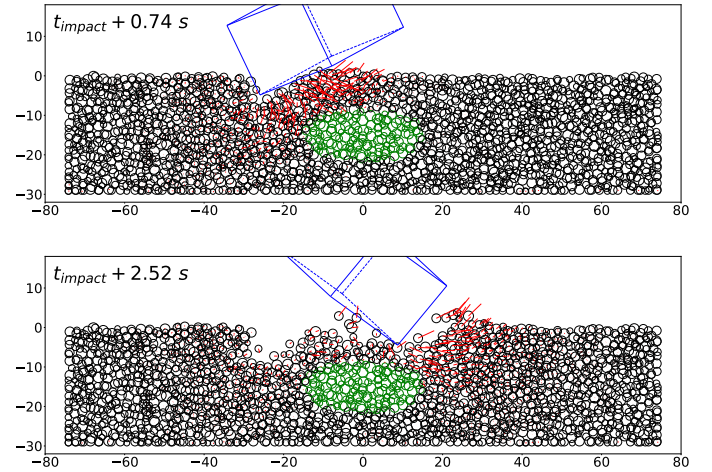


**Fig. 3.** Cross-section snapshots at two different times of MASCOT impacting the moderate-friction 30 cm regolith bed, with a buried boulder (in green), an impact angle of  $45^\circ$ , and on its back corner first. The blue cuboid represents MASCOT, and each red line indicates the projected 2D velocity of the corresponding particle.

Biele et al. (2017), showing that the excess kinetic energy (i.e., rotation and transverse linear motion) of a bouncing asteroid lander can be converted into normal linear motion; this can lead to an apparent change in the effective restitution coefficient at each bounce for multiple bounces. The impact of MASCOT on the granular bed consists of multiple bounces, and the speed ratio can thus be higher than 1 if enough rotational or transverse kinetic energy is converted into kinetic energy. In our simulations, this only occurs with a very grazing angle ( $60^\circ$ ), a 30 cm bed, and a top boulder, and the outgoing angle is about  $45^\circ$ . Even in the worst-case scenario, the vertical speed of MASCOT does not exceed the escape velocity of Ryugu, which is about  $33 \text{ cm s}^{-1}$  near the equator and about  $36 \text{ cm s}^{-1}$  near the poles. This was taken care of when MASCOT was designed (structural restitution coefficient lower than 1) and when the release was planned

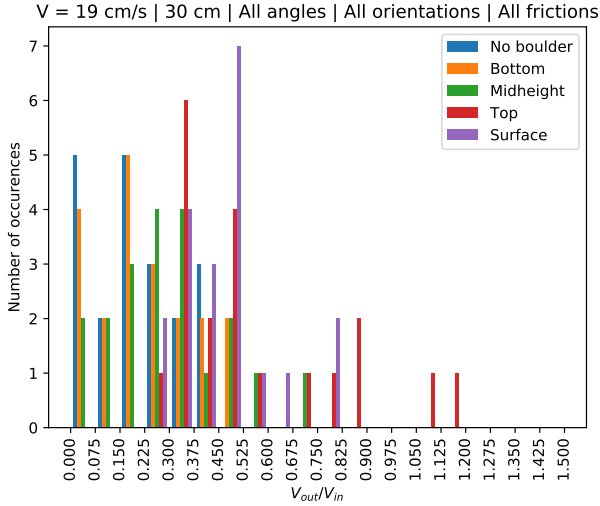


**Fig. 4.** Histogram of the outgoing-to-incoming speed ratio. Results were obtained with a 30 cm bed, two different frictions, five different angles, two different orientations, and five boulder positions.

(low initial rotational energy that could be converted into translational energy, and initial translational velocity low enough to be half the escape velocity at impact). In addition, the results are highly stochastic because MASCOT can impact different parts of the boulder according to its orientation. In the case of the surface boulder, we find similar results: high stochasticity in the results depending on where MASCOT touches the boulder, and relatively high-speed ratios.

The dependence of the speed ratios on the vertical position of the boulder is shown in Fig. 4, which confirms the trends we established earlier: a boulder increases the outgoing-to-incoming speed ratio as well as the stochasticity on average. The highest speed ratios are obtained with a top boulder and not with a surface boulder because a surface boulder can have more mobility: it is not stuck in the regolith like the top boulder, and more kinetic energy can therefore be transferred to it, resulting in a reduction of the outgoing speed of the lander compared to that obtained with a top boulder. Our results also show that even if the highest speed ratios are obtained with a top boulder, just below the surface, the average speed ratios increase with the boulder height.

Furthermore, our results show that when MASCOT directly impacts a boulder, it can lead to surprisingly low speed ratios. As shown in Fig. 4, in the case of the surface boulder, the speed ratios can reach values as low as 0.3 for several different configurations. This is due not to low restitution of energy after a single bounce in our simulations, but to the accumulation of several bounces between MASCOT and the boulder. These bounces and contacts occur at different points on MASCOT, and the behavior of MASCOT is similar to what is shown in Fig. 3. The landing process can be decomposed into several bounces and contacts, for which a certain amount of energy is dissipated each time in the boulder and in MASCOT. The combination of these multiple contacts could lead to a low overall speed ratio even if each of them is a hard contact with low-energy dissipation.

In principle, the measured low speed ratio of MASCOT should allow us to derive the dissipative properties of the Ryugu surface. Our results rather show that a low speed ratio can also result from many micro-bounces of the lander because of its geometry, between the measurements of the incoming and outgoing speeds, even if the surface by itself is a hard boulder that is not highly dissipative. We can therefore hardly infer

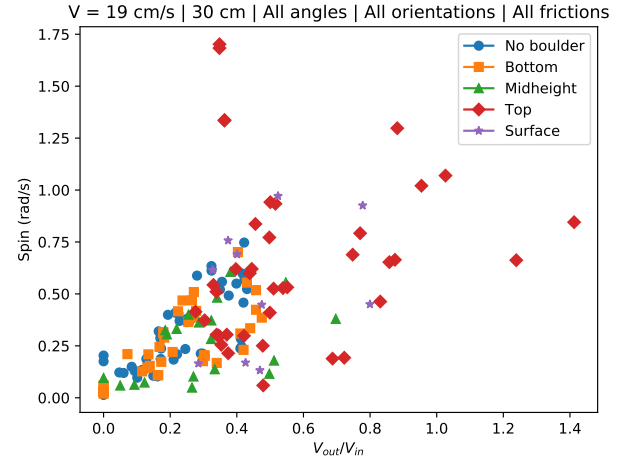


**Fig. 5.** MASCOT spin as a function of the outgoing-to-incoming speed ratio for the five angles, two orientations, two frictions, and two depths considered in this study.

the surface properties from this measurement. In future exploration, the surface dissipative properties might be better resolved with a spherical lander because this geometry favors a single bounce. The measurements of these speeds can therefore provide more reliable information about the dissipative properties of the surface.

#### (b) Spin of MASCOT

As the impact mechanism consists of MASCOT encountering resistance from the bed, pivoting, and gaining rotational energy that is then partially transformed into translational energy, it is also interesting to study the spin of MASCOT after the impact. It could be an indicator of the impact efficiency and is also an important variable for predicting the following movement of MASCOT.

Figure 5 shows the outgoing spin as a function of the speed ratio and the vertical position of the boulder. We note that in general, the higher the spin, the higher the speed ratio. More generally, the higher the boulder in the bed, the larger the range of possible outcomes in terms of speed ratio and spin. The reason for this is that the behavior of MASCOT after the impact, when it comes in contact with a boulder, can vary broadly.

Moreover, when MASCOT hits a boulder several times in a small amount of time, each contact generates a rotation opposed to the previous contact, and therefore it prevents MASCOT from gaining a higher rotation rate. By successively changing the rotation axis or the direction of rotation, MASCOT cannot pivot as fast as it does for a standard back-corner-first landing on regolith (or when impacting a boulder in a different way). This also leads to lower outgoing spin and/or speed.

#### (c) Penetration depth of MASCOT

The penetration depth corresponds to the lowest point reached by any of the corners of MASCOT in the granular bed during the collision duration. We generally find lower values with a boulder than without one. Moreover, the closer the boulder to the surface, the shallower the penetration, for the same reasons as for the speed ratio. While there is almost no difference between the speed ratios without a boulder and with a boulder located at the bottom of the bed, the penetration depth can differ by a few centimeters between these two cases.

#### (d) Trace left by MASCOT

We also investigated the depth and shape of the trace in the granular bed left by the lander after the impact in the presence

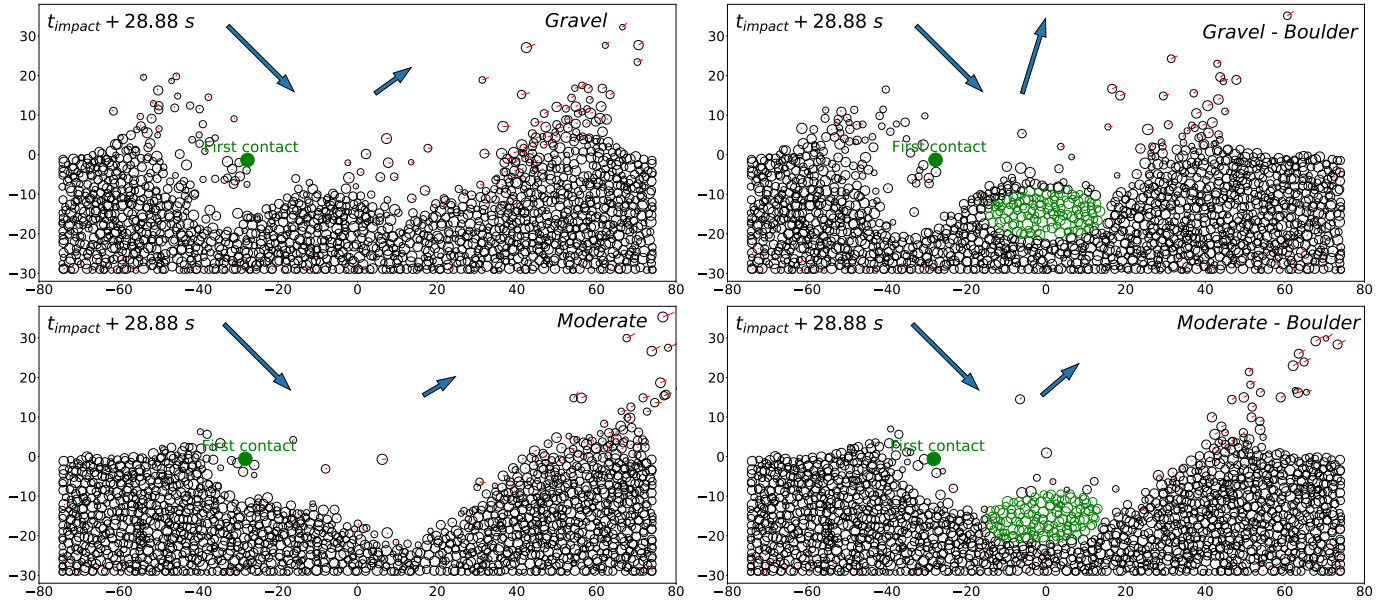


**Fig. 6.** Cross-section snapshots of MASCOT impacting different 30 cm regolith beds, with an impact angle of  $45^\circ$ , and on its back corner first. The beds differ in friction (gravel-like and moderate) and include or exclude a midheight boulder. The green aggregate represents the boulder, and each red line indicates the projected 2D velocity of the corresponding particle.  $t_{\text{impact}}$  corresponds to the simulation time when MASCOT is in contact with the regolith for the first time. The incoming and outgoing velocity vectors are indicated by the blue arrows, and the impact location is marked by the solid green circle.

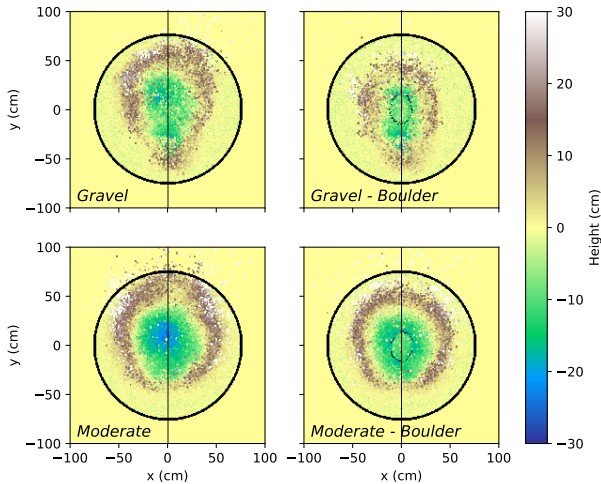


**Fig. 7.** Characteristics of the trace left by MASCOT about 29 s after having impacted different 30 cm regolith beds, with an impact angle of  $45^\circ$ , and on its back corner first. The color bar represents the height of the regolith (boulder, bed, and ejecta). The vertical black lines in the middle are the cross-section plane shown in Fig. 6, and the boulder outlines are indicated by the dotted black curves for the two boulder cases. The size of the crater is larger than the size of MASCOT, regardless of the friction and regardless of whether a midheight boulder is included or not (note that MASCOT measures 19.5 cm  $\times$  27.5 cm  $\times$  29 cm).

of a boulder. [Thuillet et al. \(2018\)](#) showed that gravel-like and moderate-friction surfaces reacted differently to the impact (deeper, more homogeneous, and more circular with moderate friction than with gravel-like friction). Here we take the case of the midheight boulder with a 30 cm deep bed to explore the effect of the boulder and the friction of the bed on the trace morphology.

In Figs. 6 and 7 the boulder is discernible from the traces for moderate-friction beds. For example, in the bottom right panel

in Fig. 7, a crown of lower heights (in blue) lies close to the center, representing the edge of the boulder. For gravel-like friction beds, even if the boulder is not discernible, the differences between no boulder and a midheight boulder are still visible. For example, ejecta opposed to the direction of MASCOT before impact are less abundant. The absence of boulders would enable MASCOT to dig more material up and to go deeper, while a boulder could restrain the particles from being pushed by the lander and remain in the crater after the impact. However, regardless of the presence of a boulder, craters obtained with moderate-friction regolith are still deeper and more homogeneous than those obtained with gravel-like grains, and the global shape of the craters is essentially the same (disregarding the boulder when present). This shows that the frictional properties of the bed have a greater effect than the presence of a midheight boulder for the morphological features of the surface after impact.

For a top boulder, if MASCOT touched the regolith bed before the boulder with one of its corners, a hole can be detected there and is due to one of the corners digging into the ground before experiencing hard resistance from the bed (due to the presence of the boulder, which decreases the mobility of the grains) or directly from the boulder. If this hole were stable, its position and depth could be a proxy for understanding how MASCOT bounced and where it is headed. However, this state is only transitory: Because the hole is deep but narrow, the bordering grains fall down the hole and fill it after MASCOT leaves. This means that few indications remain regarding the way MASCOT impacted.

### 3.1.3. Boulder at different horizontal positions

We also examined the effect of a horizontal position of the boulder, that is, a position on either the left or the right of the landing point. For the vertical position, we limited our investigation to a top boulder and a midheight boulder. Considering the size of MASCOT and the boulders, the closest edge of the boulder is

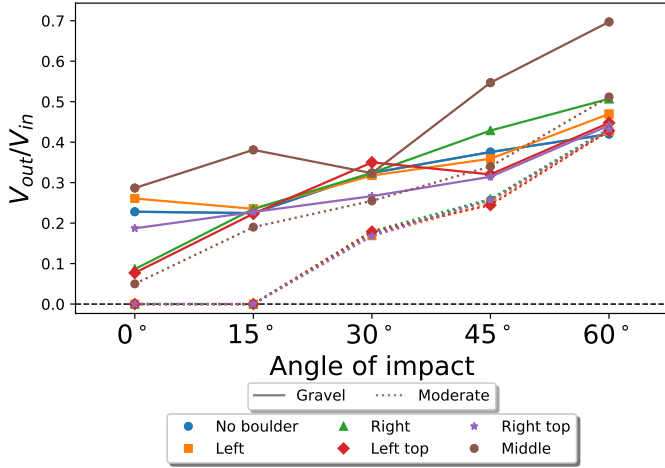


**Fig. 8.** Outgoing-to-incoming speed ratio of the lander as a function of the impact angle ( $0^\circ$  is a normal impact, and larger angles correspond to more grazing impacts), the material friction, and the position of the boulder for a 30 cm bed. The line types represent the frictional properties of the granular bed, and the symbols and colors represent the different boulder positions, as indicated at the bottom. MASCOT lands on its back corner first in these simulations. Stochasticity due to computational noise could lead to changes in the speed ratio of up to 0.1.

about 1 to 5 cm from the edge of MASCOT (in the  $x$ - $y$  plane). In Fig. 8, “left”, “middle”, and “right” apply to the midheight boulder, while “left top” and “right top” apply to the top boulder. In general, a boulder located at midheight or at the top at the left or right of the impact point has almost no effect on the speed ratio. The middle case has been discussed in previous sections, therefore we just show the midheight case as a reference.

This shows that for a boulder to have a significant effect on the outcome of the impact, it needs to be directly on the trajectory of MASCOT or just below the impacted zone. Impacting a boulder adds much stochasticity in the results, therefore it is reassuring to know for the safety of MASCOT and other landers that the zone of influence of a boulder is reduced to the few dozen centimeters above the boulder. This is true as well as for understanding trajectories and determining surface properties from landing.

### 3.2. Effect of the magnitude of gravity

Our first sets of simulations (Thuillet et al. 2018) were conducted with a gravity of  $2.5 \times 10^{-4} \text{ m s}^{-2}$ , which was the gravity of Ryugu as assumed before arrival, computed considering a simple rotating sphere approximation and the asteroid radius measured from ground-based observations by Müller et al. (2011, 2017). Hayabusa2 accurately measured the gravity to be  $1.2 \times 10^{-4} \text{ m s}^{-2}$  for the landing site, a value lower than was previously considered. We therefore investigated whether this variation in the gravity field might lead to different impact outcomes.

Figures 9 and 10 compare the outcomes with different gravity fields. The outgoing-to-incoming speed ratios and the penetration depth are very similar for the two gravity values considered here and the outgoing angles are almost the same, which leads to larger traveled distances and longer times for the lower gravity. When we consider a ballistic trajectory (i.e., gravity is the only force), half the gravity force corresponds to an increase by a factor  $\sqrt{2}$  in traveled distance and time of travel when the initial speed and angle are the same in both cases.

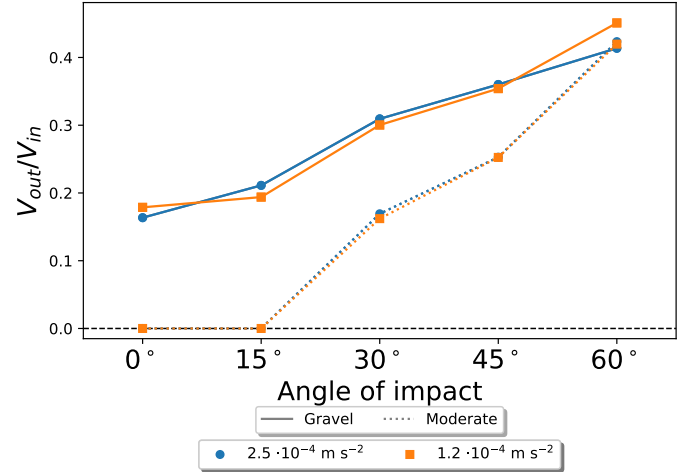


**Fig. 9.** Outgoing-to-incoming speed ratio of the lander as a function of the impact angle, the material friction, and the position of the boulder for a 30 cm bed. The line types represent the frictional properties of the granular bed, and the symbols and colors represent the different gravity fields as indicated at the bottom. MASCOT lands on its back corner first in these simulations. Stochasticity due to computational noise could lead to changes in the speed ratio of up to 0.1.

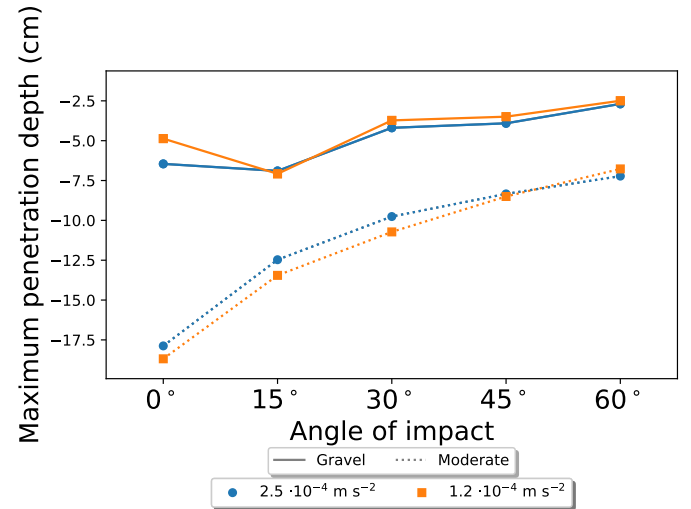


**Fig. 10.** Penetration depth of the lander as a function of the impact angle, the material friction, and the gravity for a 30 cm bed. The line types represent the frictional properties of the granular bed, and the symbols and colors represent the different gravity fields as indicated at the bottom. MASCOT lands on its back corner first in these simulations. Stochasticity due to computational noise could lead to changes in the penetration depth of up to a few centimeters.

### 3.3. Effect of the terrain slope

All previous simulations were conducted with a gravity field perpendicular to the surface. However, the surface presumably is not totally flat, and for the subkilometer-sized asteroid Ryugu, we expect many morphological irregularities. This has been confirmed by Hayabusa2. Therefore we wish to be certain that the trends established in Thuillet et al. (2018) and in this article do not depend on the slope of the terrain. The gravity of Ryugu is weak enough that it should not play any significant role in the mechanism governing the impact, but we nevertheless wish to confirm the legitimacy of this assumption. For this purpose, we need to model slopes in our simulations. One of the solutions is

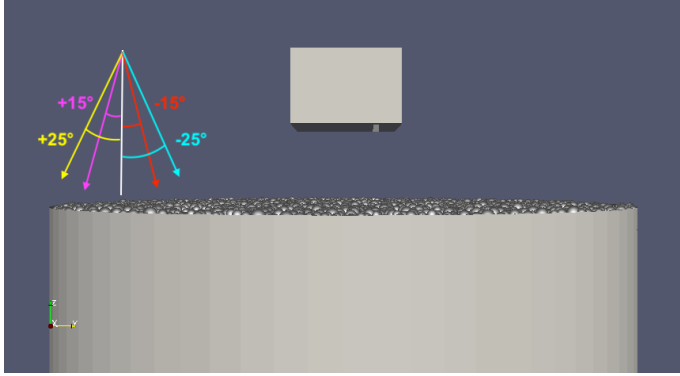


**Fig. 11.** Snapshot of MASCOT before impacting the regolith bed with the description of the different gravity angles considered in this study to represent slopes.

to generate new packings with more particles on one side and elevating the walls of the cylinder to maintain them. However, more particles lead to more time-consuming simulations, and creating such beds adds complexity. Another option is to remove enough particles from the bed to create a slope. The simulations then run even faster than previous ones, but fewer particles also means that it corresponds to shallower beds than it should have been, and direct comparisons are no longer straightforward.

The solution we chose was to change the orientation of the gravity vector, keeping of course an angle smaller than the angle of repose of both considered materials. We considered four different angles: two positive angles (+15° and +25°) and two negative angles (−15° and −25°), as shown in Fig. 11.

We adjusted the gravity vector by rotating it along the  $x$ -axis to model different slopes. This axis is normal to the velocity of MASCOT before impact, as shown in Fig. 11. Because MASCOT impacts the bed from the negative part of the  $y$ -axis (from the left side in Fig. 11 if the impact is not normal), MASCOT impacts the regolith bed on a downward slope when the angle is negative. Vice versa, when the gravity angle is positive, MASCOT impacts an upward slope. These angles are smaller in absolute values than the angles of repose of the two materials we considered: Gravel-like and moderate-friction materials have repose angles of 38.5° and 28°, respectively, which are higher than the highest considered slope of 25°. Therefore we do not expect a perturbation of the bed when the gravity is modified. As confirmation, we ran simulations without MASCOT, however, and observed the overall behavior of the particles that form the bed. Our expectations were confirmed because the bed remained in its equilibrium state.

The speed ratios for various impact angles and material frictions with different gravity angles are shown in Fig. 12 in the case of a flat impact. The effect of the slope angle is much weaker than that of other parameters such as the impact orientation and angle. There is no systematic dependence of the speed ratio on the gravity direction. The only exception is for a 15° impact angle and gravel-like friction. In this case, downward slopes lead to higher speed ratios, and the steeper the slope, the more significant the effect. However, we do not find this trend for other impact angles. Differences in the speed ratio caused by the gravity slope variation are small ( $\leq 0.1$ ), and therefore the effect of the slope angle could be concealed by the stochasticity of each impact. For the case of a moderate-friction bed, the effect of the gravity slope is negligible because a granular bed with less friction is easier to mobilize by MASCOT, regardless of the gravity slope. Moreover, for moderate-friction material, the

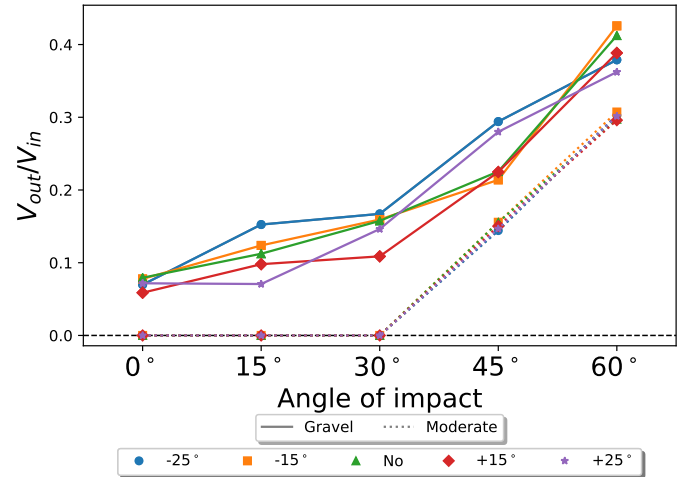


**Fig. 12.** Outgoing-to-incoming speed ratio of the lander as a function of the impact angle (0° is a normal impact and larger angles correspond to more grazing impacts), the material friction, and the gravity slope for a 30 cm bed. The line types represent the frictional properties of the granular bed, and the symbols and colors represent the different gravity slopes, as indicated in the bottom. MASCOT lands flat in these simulations. Stochasticity due to computational noise could lead to changes in the speed ratio up to 0.1.

speed ratio differences due to the stochasticity of the impact process are always much smaller than those for a gravel-like material (as found in (Thuillet et al. 2018)), which decreases the variation between different runs even more.

We also found that the post-impact velocity direction and other outcomes (such as the traveled distance and the penetration depth) also do not show notable dependence on the gravity slope. The negligible effect of the gravity slope on the results is mainly due to the very low gravity. Laboratory experiments at various gravity levels showed that more mass can be ejected from a granular bed in lower gravity for the same impact speed (Brisset et al. 2018). A highly dynamic granular bed in the low-gravity condition could also cover up the effect of the gravity slope.

In summary, these simulations show that the gravity slope has no significant effect on the MASCOT impact outcomes (at least for slopes that are gentle enough, i.e., with angles lower than the angle of repose of the material), and therefore we expect that the results we obtained for speed ratios, among others, are still valid if the lander impacts a nonhorizontal terrain.

### 3.4. Effect of the impact speed

The impact speed is loosely constrained because of the uncertainties on the shape and mass of Ryugu prior to arrival, and on the time of release of MASCOT. It is therefore important to verify whether the impact speed has a strong effect on the outcomes, such as the outgoing-to-incoming speed ratio. It is important to test the stability of our results when the impact speed changes when the trajectory is to be reconstructed, or to learn about the physical properties of the surface by studying not only the first-impact traces, but also those at the following impacts. It is also useful to investigate the traveled distances and times of travel for the different possible impact speeds (first impact and/or following impacts). Furthermore, it might be interesting to confirm whether the penetration depth in our simulations increases with the speed as given in impact cratering scaling laws.

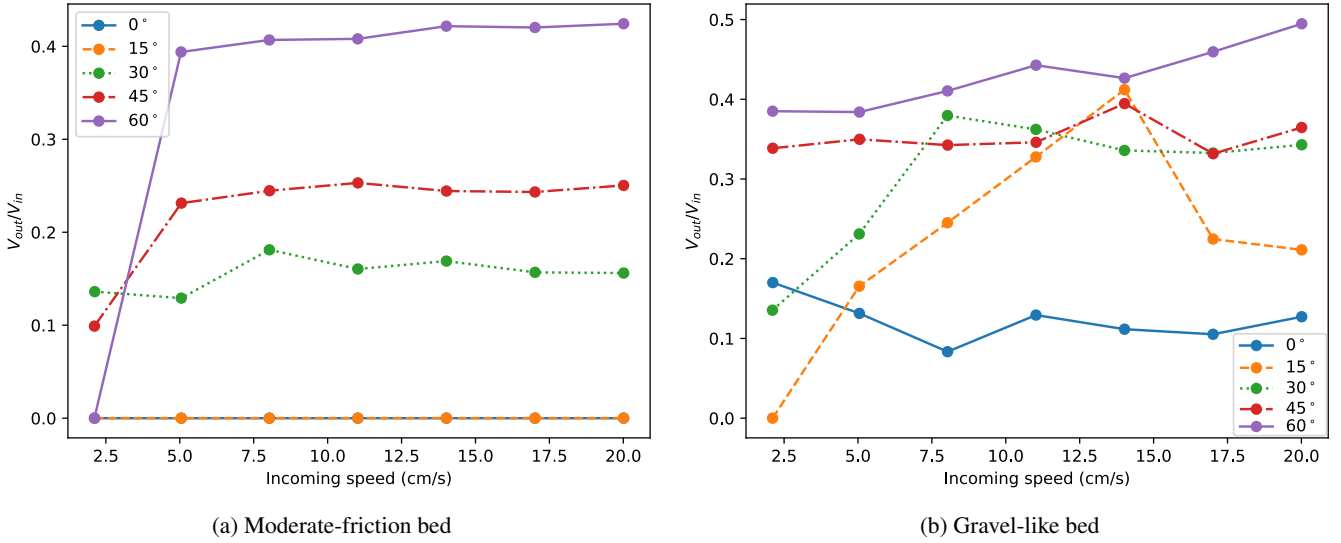


**Fig. 13.** Outgoing-to-incoming speed ratio of the lander as a function of the impact speed and angle. MASCOT lands on a gravel-like bed (*left*) or a moderate-friction bed (*right*) and on its back corner first in these simulations.

We ran simulations with different impact speeds from 2 to 20  $\text{cm s}^{-1}$ . In general, we do not expect impact speeds higher than 20  $\text{cm s}^{-1}$ , and therefore we used this speed value as a maximum. Our simulations were also conducted for different impact angles to verify whether the incoming speed has any effect on the trends we previously established (Thuillet et al. 2018).

First of all, there is a clear difference between gravel-like and moderate-friction simulations even in the evolution of the investigated outcomes as a function of impact speed. For a moderate-friction bed, the trends are much easier to establish and identify than for other dependences such as the impact angle and the depth of the bed. Concerning the outgoing-to-incoming speed ratio, the values obtained with the two frictions are shown in Fig. 13 for the five considered impact angles, different speeds, and a back-corner-first orientation.

The outgoing speed is set to 0 if the lander does not bounce (if all of its high corners do not go higher than the initial surface level); this is the case for very slow impact speeds, and therefore the lowest speed value in Fig. 13 has to be considered with caution. This may, for example, explain why the speed ratio drops to 0 in Fig. 13a for a  $60^\circ$  impact at about 2  $\text{cm s}^{-1}$ , whereas it was much closer to 0.4 for all higher speeds.

Figure 13a shows that the speed ratio is almost constant for each impact speed we considered. This means that the mechanism does not depend on the incoming speed. Moreover, as we previously stated, the speed ratio generally increases with the impact angle, and this seems to be true regardless of the incoming speed (at least for speeds higher than 5  $\text{cm s}^{-1}$ ).

However, it is much more complicated to establish a trend for a gravel-like bed. As shown in Fig. 13b, when the particles of which the bed consists have high friction, the speed ratio can be almost constant ( $45^\circ$  impact), increase slightly ( $60^\circ$  impact), or show peaks for specific speed values (e.g., the  $15^\circ$  impact at about 14  $\text{cm s}^{-1}$ ). Once again, tendencies are harder to establish for a gravel-like bed: The generally higher friction represented by the higher  $\beta$  coefficient (meaning that particles behave less like spherical particles but more like angular ones) makes the bed very sensitive to each subtle change in the impact conditions. It is therefore difficult to claim that the speed ratio does not depend on the impact speed from the gravel-like bed simulations in a general way.

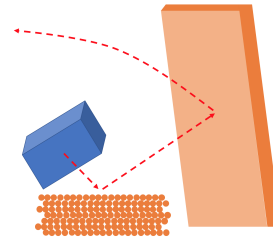


**Fig. 14.** Simplified illustration of what could have happened: MASCOT first impacts the ground and then a vertical rock, leading to an almost horizontal trajectory. The dashed red line is the potential trajectory.

### 3.5. MASCOT hitting a wall

Observations from the Hayabusa2 optical navigation camera (ONC) system and measurements from the onboard instruments of MASCOT such as the magnetometer MAG, allow us to reconstruct the trajectory of MASCOT. According to these data, MASCOT first landed on or close to a large rock, and may even have impacted a vertical part of this rock. A simple illustration of what could have happened is shown in Fig. 14, and the MASCOT trajectory can be found in Jaumann et al. (2019). Because from the images no large modification of the boulder before and after the contact with the lander can be discerned, an assumption might be that the rock was structurally strong enough to withstand the encounter without crumbling to pieces or even moving at all.

Moreover, judging from the images following the impacts, MASCOT had an almost horizontal velocity, which encourages us to argue that it first impacted the ground at the bottom of the vertical rock and then the face of the rock. In order to study this possible scenario, we ran simulations of MASCOT bouncing on the regolith bed and then impacting the rock, modeled as an unmovable rigid aggregate consisting of particles that are 2 cm in radius. In `pkdgrav`, walls cannot interact with other walls, and therefore an aggregate of particles resembling a vertical wall enables an interaction with the walls composing MASCOT. An example of the simulation of MASCOT bouncing on the regolith bed and then on the aggregate wall is shown in Fig. 15. We

**Table 2.** Minimum and maximum values for speed ratios, rotation speed, and energy ratios for MASCOT.

	$\frac{V_1}{V_0}$	$\frac{V_2}{V_1}$	$\frac{V_2}{V_0}$	$\omega_2$ (rad s <sup>-1</sup> )	$\frac{E_1}{E_0}$	$\frac{E_2}{E_1}$	$\frac{E_2}{E_0}$
Minimum value	0.116	0.155	0.019	0.138	0.014	0.024	0.0003
Maximum value	0.318	0.998	0.317	0.493	0.101	0.996	0.1006

**Notes.** The 0 index corresponds to MASCOT before the impact, 1 after contact with the regolith bed, and 2 after contact with the wall.

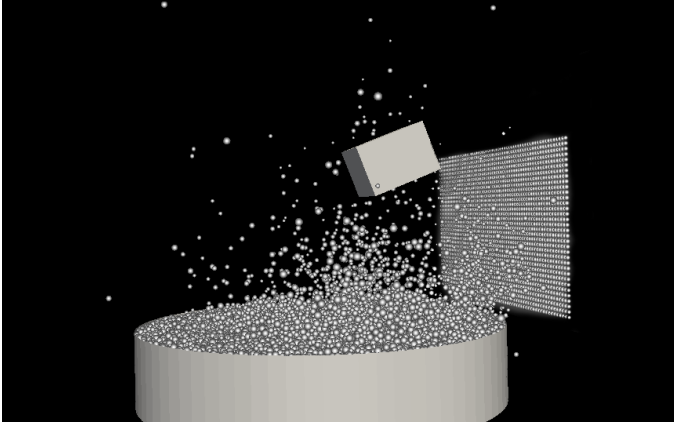


**Fig. 15.** Snapshot of a simulation of MASCOT impacting the regolith bed and then a wall consisting of a rigid aggregate of particles.

ran simulations with different angles, from 15° to 45° from the vertical, and with gravel-like friction.

The minimum and maximum values in our simulations for the outgoing-to-incoming speed ratios, rotation speeds, and energy ratios are shown in Table 2. The indices correspond to the considered instant: 0 corresponds to MASCOT prior to the impact, 1 to MASCOT just after the impact on the regolith bed, and 2 to MASCOT after the impact on the wall. We find that a second impact onto a boulder can have a wide range of energetic outcomes depending on the geometry of the impact, with a ratio of post-boulder-impact to post-surface-impact total energy,  $\frac{E_2}{E_1} \in [0.024, 0.996]$ . As we show, in some cases where one corner of MASCOT hit the granular bed first, a small fraction of its energy is lost as its linear momentum can be efficiently transferred to spin angular momentum. However, the final change in energy after two bounces (surface and boulder) lies in a narrower range,  $\frac{E_2}{E_0} \in [0.0003, 0.1006]$ , where over ~90% of the MASCOT energy is dampened. The total speed ratio can be as high as 0.317 (for the angles considered), which means that speed ratios of about 0.3 can be obtained either when bouncing on the top of a boulder, or on a regolith bed and then hitting the side of a boulder.

#### 4. Conclusion

We performed new simulations of the Hayabusa2 lander MASCOT that were begun in Maurel et al. (2018) and Thuillet et al. (2018) by expanding the parameter space and considering new setups accounting for actual MASCOT landing observations. In general, these simulations allowed improving our understanding of low-speed impacts of nonspherical objects on low-gravity surfaces, accounting for different contexts and impact geometries. Their outcomes can thus also be directly used to study phenomena other than the landing of a lander, such as the

low-speed impact of a nonspherical rock on an asteroid, and its consequences.

We first examined the effect of a boulder in the regolith bed. We found that if the boulder is buried about 15 cm below the surface, it has no effect on the outcomes of the impact. Otherwise, the higher the boulder, the higher the stochasticity, and in a general way, the higher the outgoing-to-incoming speed ratios. If a boulder is located on the side of the impact point, it has little to no effect on the bouncing behavior of the lander. We also found that landing on a rigid boulder can result in speed ratios as low as 0.3, and similar speed ratios can be obtained with a combination of bounces first on a regolith bed and then against a wall.

Moreover, we considered the actual gravity of Ryugu measured by Hayabusa2 (about half the magnitude used in our former work) and noted that the results remain unchanged. When the slope is changed (i.e., the gravity vector orientation), variations appear to be due more to stochasticity than to a real effect of the slope. This can be explained by the very low magnitude of the gravitational field.

For impact speeds high enough to allow bouncing, the speed ratio does not appear to depend on the impact speed for a moderate-friction regolith bed. However, for a gravel-like regolith, a trend is much harder to define even if a constant speed ratio is noticeable for several angles. Because the stochasticity in the gravel-like case is increased, it is difficult to be sure that the speed ratio is constant or if it increases with the impact speed.

These and previous results from Maurel et al. (2018) and Thuillet et al. (2018) can help determine or constrain the physical properties of Ryugu and of other small bodies from observations either of the trajectory of a natural or artificial impacting device with a nonspherical shape or the traces left on the surface by a low-speed impact. Observed actual particle distribution on Ryugu may be different from our assumption, and in the future, it would be interesting to consider distributions different than Gaussian. To improve the comparisons with the rocky surface of Ryugu even more, the implementation of breakable aggregates would be a significant step forward. However, setting up the value of the critical deformation leading to rupture can only be based on assumptions, and a wide range will need to be covered to explore its effect on the outcome.

Finally, the finding that a speed ratio as low as 0.3 can be reached even though the impact occurs on a solid rock has strong implications as it indicates that a low speed ratio does not necessarily imply a soft surface but can rather be due to the impact geometry and the accumulation of micro-bounces. The outcome of a low-speed impact in terms of surface properties must therefore be interpreted with caution.

*Acknowledgements.* F.T. is supported by a PhD fellowship of the University of Nice-Sophia. Y.Z. acknowledges funding from the Université Côte d’Azur “Individual grants for young researchers” program of IDEX JEDI. P.M. and F.T. acknowledge funding support from the French space Agency CNES, as well as from Academies of Excellence: Complex systems and Space, environment, risk, and resilience, part of the IDEX JEDI of the Université Côte d’Azur in connection with its Center for Planetary Origins (C4PO). Simulations were performed

at Mésocentre SIGAMM hosted at the Observatoire de la Côte d'Azur. This study was supported by the Japanese Society for Promotion of Science (JSPS) Core-to-Core program "International Network of Planetary Sciences".

## References

- Ballouz, R.-L. 2017, PhD thesis, University of Maryland, College Park, USA
- Bibring, J.-P., Hamm, V., Langevin, Y., et al. 2017, *Space Sci. Rev.*, **208**, 401
- Biele, J., Kessler, L., Grimm, C. R., et al. 2017, ArXiv e-prints [arXiv:1705.00701]
- Binzel, R. P., Harris, A. W., Bus, S. J., & Burbine, T. H. 2001, *Icarus*, **151**, 139
- Brisset, J., Colwell, J. E., Dove, A., et al. 2018, *Prog. Earth Planet. Sci.*, **5**, 73
- Capaccioni, F., Cerroni, P., Coradini, M., et al. 1984, *Nature*, **308**, 832
- Capaccioni, F., Cerroni, P., Coradini, M., et al. 1986, *Icarus*, **66**, 487
- Colwell, J. E. 2003, *Icarus*, **164**, 188
- Colwell, J. E., Sture, S., Cintala, M. J., et al. 2008, *Icarus*, **195**, 908
- Colwell, J. E., Brisset, J., Dove, A., et al. 2015, European Planetary Science Congress, EPSC2015
- de Vet, S. J., & de Bruyn, J. R. 2007, *Phys. Rev. E*, **76**, 041306
- Durda, D. D., Campo Bagatin, A., Alemañ, R. A., et al. 2015, *Planet. Space Sci.*, **107**, 77
- Fujiwara, A., Kamimoto, G., & Tsukamoto, A. 1978, *Nature*, **272**, 602
- Grott, M., Knollenberg, J., Borgs, B., et al. 2017, *Space Sci. Rev.*, **208**, 413
- Grott, M., Knollenberg, J., Hamm, M., et al. 2019, *Nat. Astron.*, **3**, 971
- Herčák, D., Auster, H.-U., Blum, J., et al. 2017, *Space Sci. Rev.*, **208**, 433
- Ho, T.-M., Baturkin, V., Grimm, C. R., et al. 2017, *Space Sci. Rev.*, **208**, 339
- Jaumann, R., Schmitz, N., Koncz, A., et al. 2017, *Space Sci. Rev.*, **208**, 375
- Jaumann, R., Schmitz, N., Ho, T.-M., et al. 2019, *Science*, **365**, 817
- Kameda, S., Suzuki, H., Takamatsu, T., et al. 2017, *Space Sci. Rev.*, **208**, 17
- Katsuragi, H., & Blum, J. 2017, *ApJ*, **851**, 23
- Katsuragi, H., & Durian, D. J. 2007, *Nat. Phys.*, **3**, 420
- Lauretta, D. S., Balram-Knutson, S. S., Beshore, E., et al. 2017, *Space Sci. Rev.*, **212**, 925
- Maurel, C., Michel, P., Biele, J., Ballouz, R.-L., & Thuillet, F. 2018, *Adv. Space Res.*, **62**, 2099
- Michikami, T., Hagermann, A., Kadokawa, T., et al. 2016, *Icarus*, **264**, 316
- Michikami, T., Kadokawa, T., Tsuchiyama, A., et al. 2018, *Icarus*, **302**, 109
- Michikami, T., Honda, C., Miyamoto, H., et al. 2019, *Icarus*, **331**, 179
- Müller, T. G., Durech, J., Hasegawa, S., et al. 2011, *A&A*, **525**, A145
- Müller, T. G., Durech, J., Ishiguro, M., et al. 2017, *A&A*, **599**, A103
- Murdoch, N., Avila Martinez, I., Sunday, C., et al. 2017, *MNRAS* **468**, stw3391
- Richardson, D. C., Quinn, T., Stadel, J., & Lake, G. 2000, *Icarus*, **143**, 45
- Richardson, D. C., Michel, P., Walsh, K. J., & Flynn, K. W. 2009, *Planet. Space Sci.*, **57**, 183
- Richardson, D. C., Walsh, K. J., Murdoch, N., & Michel, P. 2011, *Icarus*, **212**, 427
- Schwartz, S. R., Richardson, D. C., & Michel, P. 2012, *Granular Matter*, **14**, 363
- Schwartz, S. R., Michel, P., Richardson, D. C., & Yano, H. 2014, *Planet. Space Sci.*, **103**, 174
- Stadel, J. 2001, PhD thesis, University of Washington, USA
- Sugita, S., Honda, R., Morota, T., et al. 2019, *Science*, **364**, eaaw0422
- Thuillet, F., Michel, P., Maurel, C., et al. 2018, *A&A*, **615**, A41
- Tsuchiyama, A., Uesugi, M., Uesugi, K., et al. 2014, *Meteorit. Planet. Sci.*, **49**, 172
- Uehara, J. S., Ambroso, M. A., Ojha, R. P., & Durian, D. J. 2003, *Phys. Rev. Lett.*, **90**, 194301
- Van wal, S., Tsuda, Y., Yoshikawa, K., et al. 2018, *J. Spacecr. Rockets*, **55**, 797
- Van wal, S., Yoshikawa, K., & Tsuda, Y. 2019, AAS 19-243: Deployment Analysis and Trajectory Reconstruction of MINERVA-II Rovers on Asteroid Ryugu, Technical report, JAXA, Sagami-hara
- Wada, K., Grott, M., Michel, P., et al. 2018, *Prog. Earth Planet. Sci.*, **5**, 82
- Walsh, A. M., Holloway, K. E., Habdas, P., & de Bruyn, J. R. 2003, *Phys. Rev. Lett.*, **91**, 104301
- Watanabe, S.-i., Tsuda, Y., Yoshikawa, M., et al. 2017, *Space Sci. Rev.*, **208**, 3
- Watanabe, S.-i., Hirabayashi, M., Hirata, N., et al. 2019, *Science*, **364**, 268
- Yu, Y., Richardson, D. C., Michel, P., Schwartz, S. R., & Ballouz, R.-L. 2014, *Icarus*, **242**, 82
- Zhang, Y., Richardson, D. C., Barnouin, O. S., et al. 2017, *Icarus*, **294**, 98
- Zhang, Y., Richardson, D. C., Barnouin, O. S., et al. 2018, *ApJ*, **857**, 15